Femtosecond laser-induced sub-micron and multi-scale topographies for durable lubricant impregnated surfaces for food packaging applications

Karkantonis, Themistoklis; Gaddam, Anvesh; See, Tian Long; Joshi, Suhas; Dimov, Stefan

DOI:
10.1016/j.surfcoat.2020.126166

Document Version
Peer reviewed version

Citation for published version (Harvard):
Karkantonis, T, Gaddam, A, See, TL, Joshi, S & Dimov, S 2020, 'Femtosecond laser-induced sub-micron and multi-scale topographies for durable lubricant impregnated surfaces for food packaging applications', *Surface and Coatings Technology*, vol. 399, 126166. https://doi.org/10.1016/j.surfcoat.2020.126166

Femtosecond laser-induced sub-micron and multi-scale topographies for durable lubricant impregnated surfaces for food packaging applications

Themistoklis Karkantonis[1], Anvesh Gaddam[1], Tian Long See[2], Suhas S Joshi[3], Stefan Dimov[1]

[1] Department of Mechanical Engineering, School of Engineering, The University of Birmingham, Edgbaston, Birmingham, B15 2TT, UK

[2] The Manufacturing Technology Centre Ltd, Coventry, CV7 9JU, UK

[3] Department of Mechanical Engineering, Indian Institute of Technology Bombay, Mumbai 400076, India

Abstract

Adhesion of viscous liquids on packaging surfaces could lead to wastage, an increase of recycling costs, and even customers' dissatisfaction in applications related to food, cosmetics and agrochemical industries. Lubricant-impregnated surfaces (LIS) gained much attention recently over other surface functionalisation technologies due to their non-sticking response to highly viscous liquids. This work reports an investigation into anti-adhesive properties of LIS, with an emphasis on their durability. It provides an insight into the rationale design of LIS topographies in order to maximise their lubricant retention in potential food packaging applications. Femtosecond laser processing and hot embossing were employed to produce two types of topographies for LIS on stainless steel, polypropylene and polystyrene surfaces. The first type was single-scale sub-micron laser induced periodic surface structures (LIPSS), while the second one was multi-scale (MS) structures with both micron and sub-micron features. Droplet shedding characteristics of such LIPSS-LIS and MS-LIS substrates with water, milk and honey were examined under vibration and shear. The critical sliding angles at which liquid droplets attained motion on LIS were observed to be less than 32^{o} for all investigated liquids. However, the LIPSS-LIS substrates retained their functionality even after subjecting them to severe vibration, while the MS-LIS substrates partially lost their anti-adhesive characteristics. At the same time, the MS-LIS substrates exhibited premature pinning of droplets as compared to LIPSS-LIS substrates, under shear forces. Both vibration- and shear-induced loss of lubricant impacted the MS-LIS functionality.

Keywords: Food packaging, femtosecond laser, laser induced periodic surface structures, lubricant-impregnated surfaces, superhydrophobic surfaces, surface texturing

1. Introduction

Annually, around 1.3 billion tonnes of food is wasted during the production, distribution and consumption stages, which has a tremendous impact on both economy and environment [1]. Although food waste occurs at all stages of the supply chain, private households represent a large fraction of this [2-3]. At the same time, a significant share of the food wastage in households is due to difficult-to-empty packaging, where the viscous food adheres to packaging surfaces. For example, it is estimated that 15% of the wastage in households is due to adherence of high-valued foods, such as yogurt, to the packaging surfaces [4-5]. Residual food on surfaces of the packaging also leads to an increase in cleaning cycles and recycling costs [6]. Furthermore, adhesion of viscous substances to process equipment such as pipework and mixing vessels in food industries also leads to cross-contamination, increased water load, and microbial growth [7]. Therefore, it is essential to design surfaces with anti-adhesive characteristics which are robust and durable. Such anti-adhesive surfaces that can minimise the adhesion and accelerate the mobility of various viscous liquids are of great importance to the food, cosmetic and agrochemical industries.

At large, anti-adhesive surfaces targeting food packaging can be achieved by two surface functionalisation approaches. In the first, coatings based on fluorine and silicone can be applied on packaging surfaces to lower their surface energy, thus imparting their hydrophobic and oleophobic properties. However, the negative effects of long chain perfluorinated compounds such as PFAS and PFOS on human health and environment have inspired efforts to develop alternative methods to lower the surface energies of materials [8]. Regarding the second approach, the surfaces are textured to produce micro/nanoscale topographies that induce Cassie-Baxter state. The entrapment of gas into micro/nanoscale cavities on such textured surfaces results in high contact angles, thereby resulting in superhydrophobic and superoleophobic characteristics. However, the wetting transitions due to dissolution of gas into interacting liquids [9], moderate liquid pressure [10] and surface chemistry [11] affect their long-term durability in practice. At the same time, not all superliquiphobic surfaces with relatively high contact angles necessarily shed liquids from surfaces due to high contact angle hysteresis (CAH). Thus, such surface functionalisation techniques have their own shortcomings that make them not ideal for non-stick food packaging applications.

A relatively new surface functionalisation technique based on lubricant impregnation of micro/nanotextured surfaces has gained much attention recently. Lubricant-impregnated

textured surfaces (LIS) that are inspired by the Nepenthes pitcher plant can offer extremely low CAH and thus to shed liquids away easily without any adhesion. Based on the current practices, the requirements in producing LIS are: (i) the micro/nanotextured surfaces to retain the lubricant; (ii) the utilised lubricant and the repelling liquid should be immiscible; and (iii) the solid/base surface should be wetted by the lubricant instead of repelling it [12]. Due to their stability against wetting transition and very low CAH, LIS capabilities are extensively investigated for applications related to drag reduction [13-14], fog harvesting [15], anti-biofouling [16-17] and anti-frosting [18]. However, simple Newtonian liquids, especially water, were mostly investigated in the reported research.

Most of the liquid foods are composed of fats, stabilizers, surfactants and emulsifiers and therefore exhibit non-Newtonian behaviour. These components make the interaction of liquid foods with surfaces significantly different from that of water. Several investigations were reported recently that were focused on the interaction of complex liquids with LIS, aiming to achieve fouling-resistant and easy-to-empty packaging. Zhang et al. [19] employed sol-gel and hydrothermal methods to impregnate nanoporous Aluminium surfaces and demonstrate their ant-wetting characteristics against various liquid foods. Lee et al. [20] prepared LIS employing nanotextured Aluminium substrates and investigated their anti-adhesive characteristics. They showed that non-connecting topographies can retain their non-sticking nature better than the connecting topographies even after subjecting them to continuous shear forces. Zouaghi et al. [21] demonstrated that LIS prepared using hierarchical textures produced through ultrashort laser processing of stainless steel could reduce dairy fouling compared to some reference superhydrophobic surfaces. Several other studies focused on preparing LIS on glass and silicon-based substrates examined their non-wetting properties when in contact with complex liquids [22-27]. Although most of these studies involved textured metallic and glass substrates, it should be noted that polymers are predominantly used as food packaging materials. In this regard, Mukherjee et al. [28] used oil absorbent polyethylene films to prepare LIS and demonstrated their anti-adhesive characteristics towards viscous liquid foods, such as ketchup and yoghurt. Recent investigations reported anti-adhesive properties of thermoplastic-based LIS prepared through solvent casting when in contact with liquid foods and detergents [29-30].

In summary, a significant progress was made in developing LIS for shedding complex liquids away from surfaces. However, few investigated LIS on thermoplastic materials that are of interest to food and cosmetic packaging industries. At the same time, durability aspects of LIS were not sufficiently studied while they are critical for their broader use. Since the LIS

properties are shown to deteriorate quickly under liquid shear [31-32] and vibrational forces [33], it is important to understand the effects and impact of LIS topographies on their durability. Furthermore, the process chains employed in the reported research for producing LIS, especially their underpinning micro/nanoscale topographies, are not an industry practice in food and cosmetic packaging applications, e.g. the use of LIS in producing containers, bottles, caps and various food and cosmetic handling equipment.

This research reports an investigation into the LIS properties achieved on sub-micron and multiscale topographies produced by employing metallic replication masters. The masters were textured by using ultrashort laser processing and then their topographies were replicated on commonly used food packaging thermoplastics, i.e. polystyrene and polypropylene, through hot embossing. Thermoplastic surfaces were impregnated with a silicone oil and their anti-adhesive response to three liquids, i.e. water, whole milk and honey, were investigated. In addition, durability tests were conducted on LIS samples with two types of topographies, in particular, sub-micron and multiscale ones, to study and compare their lubricant retention capacities under vibration and shear loading.

2. Materials and methods

2.1 Fabrication of sub-micron textured metallic moulds

Commercial X6Cr17 ferritic stainless steel (SS) plates with dimensions 30 x 20 x 0.7 mm and an average roughness (S_a) of 35 nm were used to produce on them two types of surface topographies. The SS substrates were textured at atmospheric conditions using an ultrafast Ytterbium-doped laser source (Satsuma, Amplitude Systems). The laser source has the following technical specification: a pulse duration of 310 fs at a nominal wavelength of 1030 nm and pulse repetition rate (f) up to 500 kHz with an average power (P) of 5 W. The laser texturing experiments were carried out on LASEA LS5 machine and its beam delivery system is shown in Fig. 1a. It was equipped with a 3D scan head mounted on a Z-axis stage and a telecentric focusing lens with 100 mm focal length to steer a linearly polarized Gaussian beam across the substrates with a maximum scanning speed (v) of 2000 mm/s. In addition, a high precision stack of two rotary and two linear stages was used to position the substrates inside the machine working envelope. The SS substrates were processed with a constant scanning speed of 1000 mm/s and a spot diameter (2Ω) of 35 μm at the focal plane.

A horizontal raster scanning strategy was implemented to fabricate laser induced periodic surface structures (LIPSS) with sub-micron ripples. At the same time, a grid-like scanning

strategy with multiple (40) scans was employed to produce multiscale structures (MS) that included a combination of micron and sub-micron scale features. These two scanning strategies are illustrated in Figure 1(b). In order to obtain highly regular LIPSS, trials were conducted by varying the hatch distance (h) between two consecutive lines and also the average power at a repetition rate of 250 kHz. A similar strategy was adopted for obtaining the MS topographies, however, a repetition rate of 500 kHz was used in this case. The overlap (O) between pulses and the pulse fluence (φ_0) were calculated using the expressions reported in another research [34]. The optimised laser processing parameters used to produce the two topographies, i.e. LIPSS and MS ones, over an area of 30 x 20 mm^2 on the SS substrates are given in Table 1. The processing time for producing the LIPSS and MS topographies were 2 and 10 minutes, respectively.

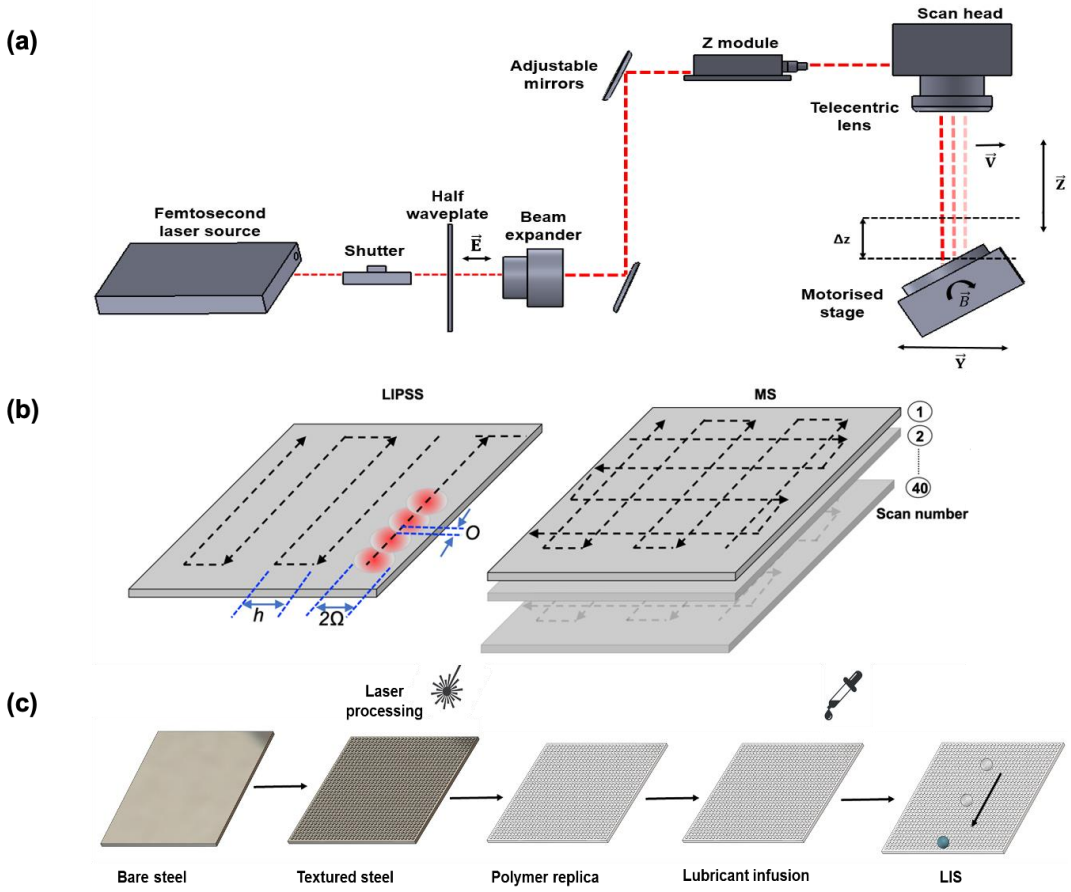

Figure 1. The experimental set-ups: (a) a schematic of the used beam delivery system; (b) two scanning strategies for fabricating LIPSS (left) and MS (right) topographies; (c) an illustration of the process chain used to produce LIS.

Table 1. Optimum laser processing parameters for LIPSS and MS topographies.

Structure	f (kHz)	φ_0 (mJ/cm^2)	h (μm)	v (mm/s)	Number of scans	Scanning Strategy	Polarisation
LIPSS	250	210	5	1000	1	Horizontal	Linear (s)
MS	500	430	40	1000	40	Grid	Linear (s)

2.2 Polymer micro/nano replication and LIS preparation

The LIPSS and MS topographies on the SS plates were replicated onto polystyrene (PS) and polypropylene (PP) thermoplastic sheets (Alfa Aesar) of 1.6 mm thickness. In particular, a hot embossing set-up with a controllable hotplates' temperature and load was used to replicate the LIPSS and MS topographies on the sheet surfaces. During the replication process, the textured SS plates together with the blank thermoplastic sheets were placed between the hotplates and a pre-determined load was applied, and a temperature greater than the glass transition temperature of the thermoplastics was maintained for 5 minutes. To achieve as high as possible replication quality and samples' flatness, the operating temperature and load were optimised for the two thermoplastic materials used in the experiments. The optimised process settings together with the material properties are provided in Table 2.

Most of the reported studies employed perfluorinated oils [19-21, 23-24, 26, 29-30], essential and vegetable oils [27-28], and silicone oils [22, 25] as lubricants to demonstrate the LIS capabilities in food packaging applications. Although perflourinated oils are extensively used, such lubricants release fluorine similar to that of fluorinated coatings and therefore pose considerable health risks [35]. At the same time, essential and vegetable oils exhibit a strong aroma and also are not compatible with all liquid foods [36]. On the other hand, sufficient regulation standards are available for silicone-based lubricants as food additives [37] and therefore the silicone oil was selected as a lubricant in this study. Prior to the fabrication of LIS, all SS and thermoplastic replicas were cleaned with isopropyl alcohol to remove any surface debris or contamination. A silicone oil (Sigma-Aldrich) with 20 cSt viscosity at 25 °C was used as a lubricant. It was pipetted onto the textured SS and thermoplastic substrates for impregnation in the textures. The wetting and spreading of lubricant on micron and/or sub-micron scale cavities of textured substrates is mediated by the capillary length (l_c), which is expressed as $l_c = (\gamma/\Delta\rho g)^{1/2}$ [38]. Here, γ (= 20.6 mN/m) is the surface tension between the

silicone oil and air, $\Delta\rho$ (= 949 kg/m^3) is the density difference between silicone oil and air and g (= 9.81 m/s^2) is the gravitational constant. Consequently, the characteristic capillary length for silicone oil is approximately 1.5 mm. Since the length scale of MS and LIPSS topographies is much less than the characteristic capillary length, the capillary forces aid in wetting and spreading of silicone oil. After the textured substrates were completely wetted by the silicone oil, they were stored in a vacuum chamber for 15 minutes. The mild vacuum has further accelerated the impregnation process by releasing the entrapped air from sub-micron cavities. Thereafter, the LIS substrates were kept vertically for an hour, in order to drain any excess lubricant from the surfaces with the help of gravity. A schematic illustration of all the process chain steps used to attain LIS is provided in Figure 1(c).

Table 2. Material and processing conditions for hot embossing of PS and PP replicas.

Material	Load (kN)	Embossing Temperature (°C)	Melting temperature (°C)	Glass transition temperature (°C)	Hold time (min)
PS	0.16	100	240	100	5
PP	0.26	115	170	-10	5

2.3 Surface characterisation

The two surface topographies on SS and thermoplastic substrates were characterised using a scanning electron microscope (SEM, JEOL JCM-600). A focus variation microscope (Alicona G5) was used to analyse the micro-scale topographies of the MS substrates. Whereas, an atomic force microscope (AFM, MFP-3D, Asylum Research) was used to analyse sub-micron features of LIPSS and MS topographies. The 2D-FFT analysis was conducted using Gwyddion open-source image analysis software to obtain the LIPSS orientation and periodicity. The wettability of as-received SS and thermoplastic sheets, textured SS and thermoplastic replicas and LIS was investigated by measuring the water contact angle of 5 µL droplets using a goniometer (Attension Theta, Biolin Scientific). Following this, the contact angle hysteresis (CAH) was evaluated using the tilting stage of the goniometer. In particular, the advancing and receding contact angles were measured during the initiation of droplet movement when the substrate was tilted at an angle.

Furthermore, the critical sliding angle (CSA) of droplets was measured on as-received SS plates and thermoplastic sheets, textured SS plates and replicas and LIS. Three test liquids, i.e. water, whole milk and honey, were used to investigate the LIS response. 15 µL droplets of each

test liquid was pipetted onto the LIS samples to observe the droplet motion. The droplet movement on the surfaces was recorded using a motorised tilt stage with a positional accuracy of 10 arc seconds and a digital camera (Canon 2000D). To avoid any droplet impact on the sample surfaces, the pipette was held in a fixture very close to the surface of the samples. The distance between the tip of the pipette and sample surfaces was maintained at less than 2 mm. For each test run, five measurements were taken by placing droplets at different locations on the sample surfaces and the average CSA values were analysed.

2.4 LIS durability analysis

At the end of the food supply chain, the packaged food is transported to the retailers and ultimately to the households. During these stages, the packaging containers would be subjected to vibration. At the same time, the packaging surfaces would be also subjected to shear loads when liquid foods would be taken out/emptied from their containers by end-users. To account for these different types of loads, two tests were conducted to evaluate the durability of the thermoplastic LIS. First, the LIS samples were placed inside a container filled with water and were subjected to vibration with 50 Hz frequency for 5 minutes. Thereafter, the shedding characteristics of the LIS samples were re-examined by measuring CSA of water, whole milk and honey droplets on vibrated surfaces. The amount of the lubricant retained by the samples after their exposure to vibration was evaluated by measuring the mass of samples before and after the tests using a precision weighing balance. Secondly, the thermoplastic LIS samples were tilted at an angle of 15^{o}, and the whole milk and honey droplets of 15 μL were deposited on a single track of the surface. The camera was used to record the droplet motion at 50 frames per second. The droplets of the test liquids were continuously dripped on the LIS samples until their motion was observed to stop. Each test run was conducted three times. Thereafter, the recorded videos were post-processed using "Tracker" video analysis software to evaluate the steady-state velocity of the whole milk and honey droplets on LIS samples. Finally, adhesion characteristics were also investigated by immersing the LIS samples into containers with milk and honey for up to 50 times.

3. Results and discussion

3.1 Analysis of surface topographies

Since regular and periodic textures allow a better understanding of liquid-surface topography interactions, the first efforts were focused on producing highly regular, periodic LIPSS and MS topographies on SS substrates. To minimise the effect of the Gaussian beam, a high overlap

scanning strategy was adopted and thus to achieve highly regular LIPSS [39]. A pulse overlap fixed at 70%, the pulse fluence and the hatch distance were varied from 50 to 300 mJ/cm^2 and from 1 to 6 µm, respectively. As a result, the accumulated fluence per area from 1.5 – 53.3 J/cm^2 was attained. While different structures such as uniform ripples, a combination of ripples and roughness, and discontinuous ripples were observed in the investigated parameter domain, the highly regular LIPSS were obtained at accumulated fluence of 7.4 J/cm^2.

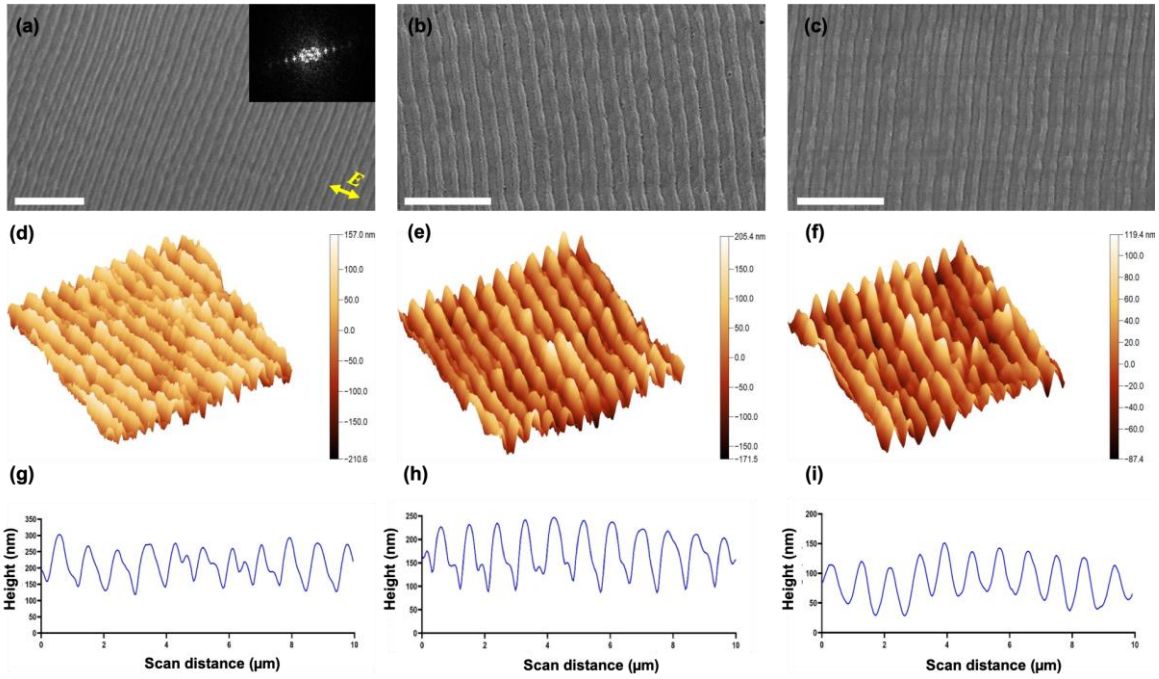

Figure 2: The surface topography analysis of LIPSS substrates: **(a-c)** SEM micrographs SS, PS and PP substrate, respectively with a 2D-FFT image inset in (a); **(d-f)** AFM micrographs of SS, PS and PP substrates, respectively; **(g-i)** plots showing height profiles of SS, PS and PP substrates, respectively.

At the same time, to produce the MS topographies, in particular consisting of microscale pillars with superimposed sub-micrometre features, the hatch distance was varied from 25 - 50 µm while the number of scans from 5 to 40 at a fixed average power. The grid-like scanning strategy led to a higher accumulated fluence at the intersecting points and therefore valleys and bumps were formed on the surface. A topography with minimum surface defects, such as sporadic pits and roughness, was obtained with an inter-pillar spacing of 40 µm and a height of 10 µm. Although no surface defects were observed when a small number of scans were used, the height of the pillars was not sufficient to distinguish the resulting MS topography from that of the single scale LIPSS substrates. Therefore, the MS replication master was produced with

40 scans as stated in Table 1. The LIPSS and MS masters were fabricated over the SS plates with the optimised settings in Table 1 and then replicated on thermoplastic sheets as explained previously.

The SEM micrographs of highly regular LIPSS on SS, PS and PP substrates are shown in Figs. 2a, b and c, respectively. The LIPSS were formed with an orientation normal to the beam polarisation vector (*E*) (see Fig. 2a). The clearly defined 2D-FFT (the inset in Fig. 2a) signify a high regularity of the fabricated LIPSS. Furthermore, the periodicity was evaluated to be in the range from 800 to 900 nm based on the SEM and 2D-FFT characterisation results that were less than the wavelength of the femtosecond laser and similar to that reported by other researchers [40-41]. The respective 3D AFM micrographs of highly regular LIPSS on SS, PS and PP substrates are provided in Fig. 2d, e and f and they depict a high replication quality. The AFM profiles (see Fig. g-i) show a mean height from 100 to 200 nm on all substrates. Furthermore, it is evident from the comparison of LIPSS average height on SS, PS and PP substrates at different locations over a scan length of 10 µm that a high replication performance was achieved, especially greater than 90%.

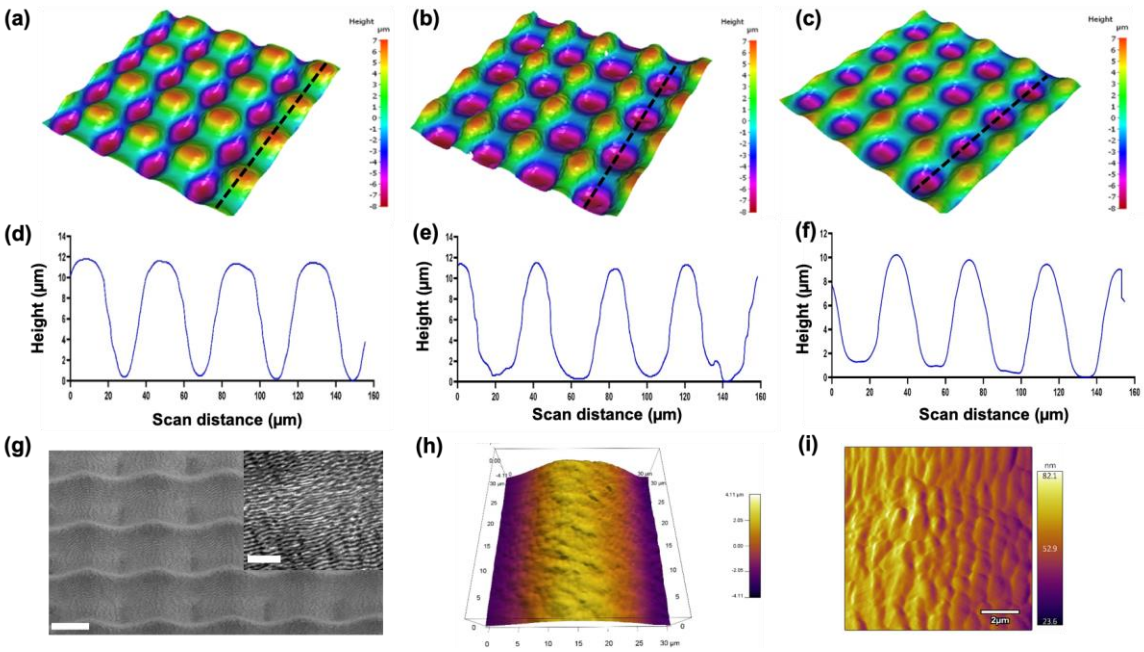

Figure 3: The surface topography analysis of MS substrates: **(a-c)** the 3D micrographs of SS, PS and PP substrates, respectively; **(d-f)** plots showing height profiles on SS, PS and PP substrates; **(g)** the SEM micrograph of SS topographies (scale bar: 20 µm) with a magnified

view of sub-micron features on pillars in the inset (scale bar: 5 μm); **(h-i)** the AFM micrographs showing sub-micron features on top of the pillar of PS and PP replicas, respectively.

The 3D micrographs of MS topographies on SS, PS and PP substrates are shown in Figs. 3a, b and c, respectively. The micrographs depict the negative patterns of the MS topography on SS surface that are then replicated on thermoplastic sheets. Furthermore, the height profiles of microscale pillars on both SS and thermoplastic substrates as shown in Fig. 3d-f where also the achieved replication performance of more than 95% is evident. The SEM micrographs in Fig. 3g depict sub-micron scale features superimposed on microscale pillars. Again, the replication quality of sub-micron features on thermoplastics replicas was assessed by analysing AFM micrographs taken on the top of the micro-scale pillars. It is evident that the sub-micron features were replicated on the PS MS samples as shown in Fig. 3h. A magnified view of sub-micron features of a PP MS samples is provided, too, in Fig. 3i and again it depicts a high replication performance. The AFM measurements of SS and thermoplastic samples show that the height of sub-micron features was in the range from 50 to 100 nm, which was substantially less than that achieved on the LIPSS samples (see Fig. 3g-i).

3.2 Wettability characterisation

The average static water contact angles (CA) measured on as-received, textured and LIS of SS, PS and PP substrates are provided in Fig. 4a. Initially, textured SS substrates exhibited hydrophilicity, in particular, CA of 88.2^{o} and 67.5^{o} on LIPSS and MS samples, respectively. However, CAs significantly increased over a period of two weeks to reach the respective values of 113^{o} and 138^{o}. This can be explained with the exposure of laser textured SS substrates to the ambient environmental conditions and the accumulation of carbon from CO_2 decomposition on surfaces that lowered the surface energy as reported in previous research [42-43]. It is important to stress that the CA measurements on thermoplastic substrates were stable over the same time period of 2 weeks. The combined alteration of surface chemistry and topography was the reason for the CA increase on textured SS substrates. On the other hand, only the alteration of topography has caused the change in CA on inherently hydrophobic thermoplastic substrates. The MS topographies substantially increased the contact angles (CA > 130^{o}) on SS plates and their PS and PP replicas, whereas the influence of highly regular LIPSS on thermoplastic replicas was marginal.

At the same time, the LIPSS and MS topographies did not have any influence on CAs of lubricant-impregnated surfaces of SS and thermoplastics. However, a slight difference in the values of CA for LIPSS-LIS and MS-LIS of SS substrates is evident in Fig. 4b when compared

to their LIS counterparts on thermoplastic substrates. In general, a droplet on LIS can assume a shape in any of the 12 possible thermodynamic states, which is determinted by the spreading coefficient of the lubricant on a substrate in the presence of water [12]. The noticeable difference in the CA values on LISs of SS substrates could be attributed to the appreciable difference in the spreading coefficients of LIPSS-LIS and MS-LIS. However, a further investigation is needed to explain the effects of the substrate material on the observed droplet shape on LIS. The images of water droplets on textured and LIS substrates are shown in Fig. 4b. The wetting ridge formed by the water at the periphery of the water droplet on LIS can be seen in the figure. Furtheremore, the CAH of water droplets was measured to be less than 5^{o} on all the LIS.

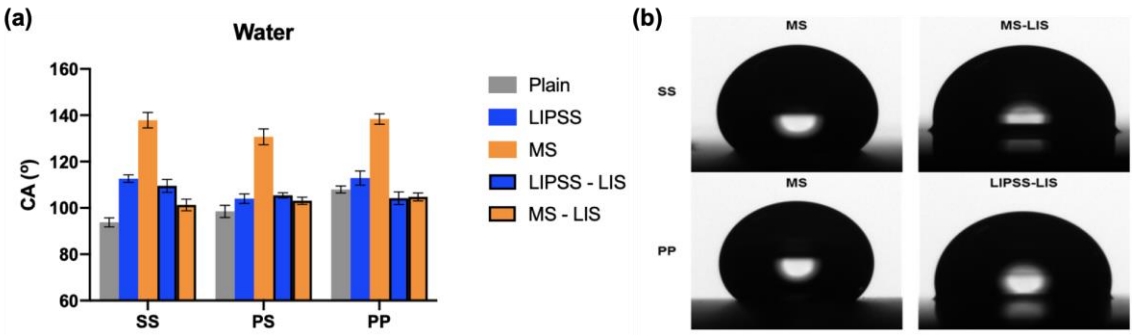

Figure 4. The water CA measurements obtained after two weeks: (a) static water CA on as-received, textured and LIS topographies of SS, PS and PP substrates; (b) Images of the water droplet on textured and LIS of the SS and PP substrates.

Subsequently, the shedding behaviour of water, milk and honey droplets was characterised by measuring the critical sliding angle at a droplet motion was initiated. Droplets of the test liquids on SS and PS LIS surfaces are shown in Fig. 5d. It should be noted that the water and milk droplets were dyed for better visibility. The average CSA for all test liquids on as-received, textured and LIS topographies of SS and thermoplastic substrates are shown in Fig. 5a, b and c. The as-received and textured surfaces of the SS substrates pinned the test liquids even after the substrates were tilted at 90^{o}. At the same time, some droplet motion was observed at CSA of less than 40^{o} on as-received thermoplastic surfaces for all test liquids. However, the droplets were observed to have sagged while sliding along the thermoplastic surfaces, leaving behind traces of test liquids as shown in Fig. 5d. Interestingly, the surface texturing on thermoplastic surfaces did not aid the droplet movement. In fact, the droplets were either pinned to the MS surfaces (see Fig. 5d) or CSA increased to more than 70^{o} and 60^{o} in the case of water on LIPSS PS and PP substrates, respectively. The lubricant infiltration into the textured surfaces

dramatically reduced CSA on all substrates as shown in Fig. 5a-c. The mobility of the droplets on LIS regardless of the liquid type was aided by a slippage at the contact line and also the hemispherical shape of the droplet was preserved as shown in Fig. 5d. For most of the experimental domain, CSA was observed to be less than 10^{o}, except milk droplets on PS surfaces (CSA < 32^{o}).

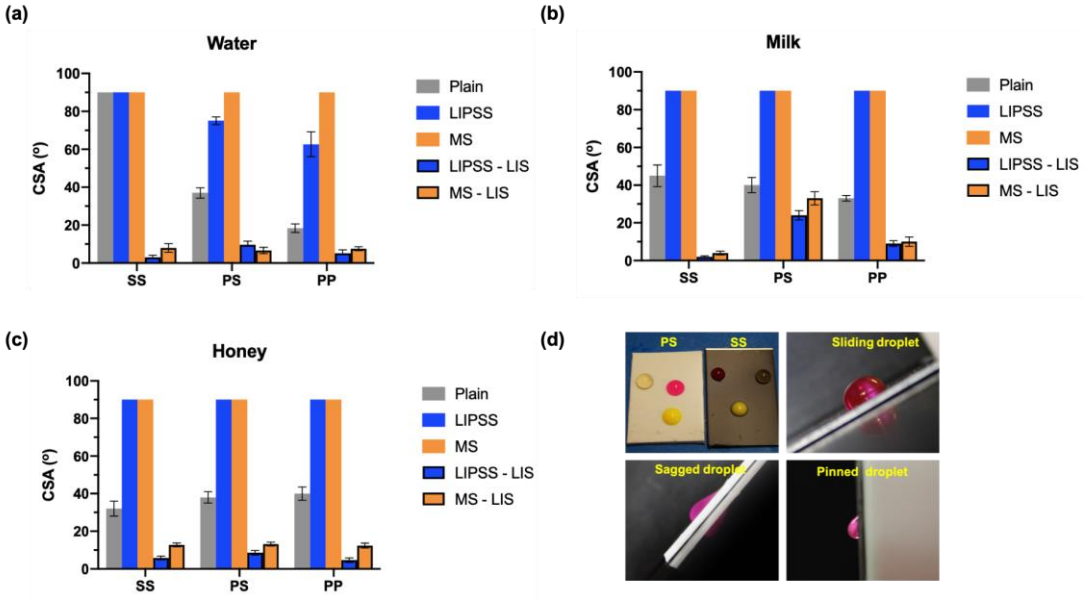

Figure 5. CSA on as-received, textured and LIS topographies of the SS, PS and PP substrates for: **(a)** water, **(b)** milk and **(c)** honey droplets. **(d)** An image of water, milk and honey droplets on the MS-LIS surfaces of PS and SS samples together with different droplet shedding behaviours is shown.

3.3 Durability characterisation of LIS

3.3.1 Vibration assessments

A critical durability characteristic of LIS is their liquid shedding performance, especially the functional lubricant retention capacity of textured surfaces in the context of this research. Therefore, the durability of LIS substrates was examined by subjecting them to vibration. LIS of SS and thermoplastic substrates were agitated by using a standard laboratory vortex mixer for 5 minutes as shown in Fig. 6a. The amount of lubricant retained after the vibrations was assessed by measuring the substrate mass at fixed intervals of time. In particular, the lubricant locked into the sub-micron cavities of LIPSS substrates was too small to lead to any noticeable changes in the substrates' mass. However, this was not the case for the MS topographies and considerable changes in the substrates' mass were observed after the vibration tests. The Fig.

6b shows the amount of lubricant retained by PS and PP MS topographies with the increase of time they were subjected to vibrations. As can be seen, a large amount of lubricant was lost within a minute after subjecting the substrates to vibration. Overall, the MS topographies on the PP and PS substrates retained only approximately 20% and 40% of the lubricant, respectively, and reached their plateaus after subjecting them to only 2 min vibrations. The lubricant retention on these substrates can be attributed to the high capillary forces due to sub-micron cavities on both LIPSS and MS topographies. At the same time, the substantial vibration-induced loss of lubricant from microscale cavities onto the MS topographies can be explained with reduced capillary forces as depicted in Fig. 6c.

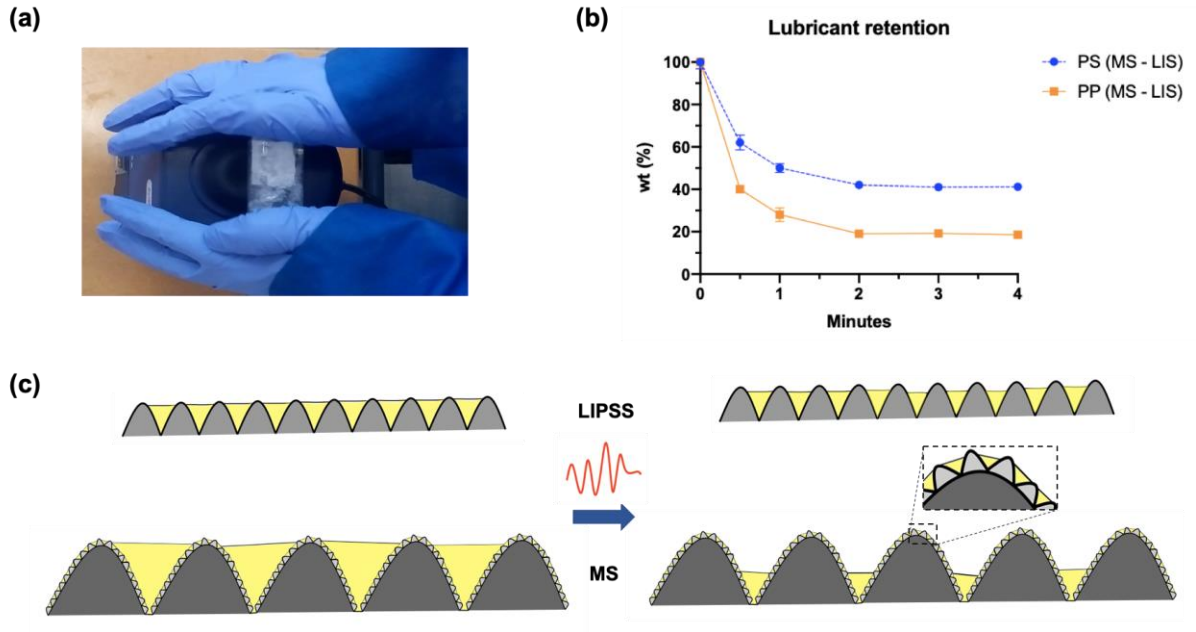

Figure 6. An investigation into the lubricant retention capacity of LIS: **(a)** the experimental setup used for subjecting LIS substrates to vibration; **(b)** the lubricant retention capacity of MS topographies on the PS and PP substrates with time; **(c)** an illustration of vibration-induced loss of lubricant infused into LIPSS and MS topographies.

In addition, CSAs of droplets from the same test liquids as those investigated in Section 3.2 were measured on LIS substrates. Fig. 7a shows the CSA change on LIS substrates before and after subjecting them to vibrations for 5 minutes. Large CSA changes were observed on MS topographies of both SS and thermoplastic substrates, while only marginal changes were noticed on LIPSS. The lubricant depletion of MS topographies on SS substrates even led to pinning of the water droplets to the surface and thus the anti-adhesive functionality was

completely lost. The milk droplets had shown a similar behaviour as depicted in Fig. 7b. However, despite detecting a droplet sliding on MS-LIS topographies, the milk droplets left small 'satellite' droplets behind on the surfaces as shown in Fig. 7d. Thus, a partial loss of functionality was evident with the milk droplets on MS topographies after subjecting them to vibration. A similar phenomenon with viscoelastic droplets on superhydrophobic surfaces was previously reported [44]. Fig. 7c shows the sliding behaviour of honey droplets on the LIS surfaces before and after vibration. Contrastingly, the loss of functionality on MS topographies in regards to the honey droplets was much less compared to that observed with water and milk droplets. However, this can be attributed to the higher density and viscosity of honey in comparison with water and milk that led to an altered surface response as a result of a different balance between the forces of gravity, viscosity and contact line pinning. For a profound understanding of the sliding behaviour, the rheological properties of the considered test liquids should be elucidated by correlating non-dimensional parameters of these forces [45], however, such a study is outside the scope of this research.

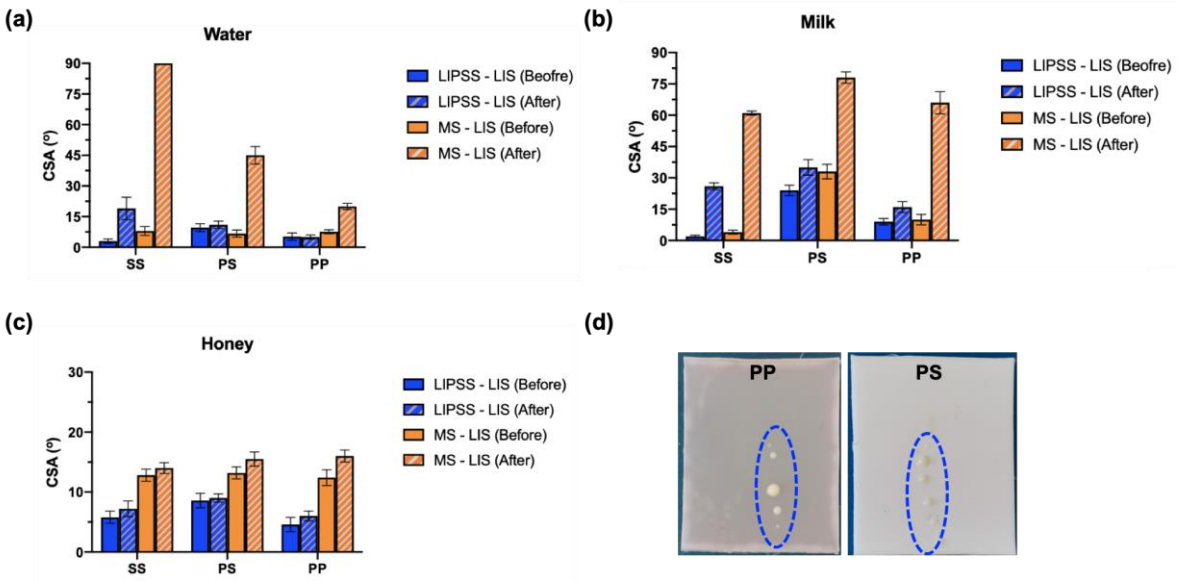

Figure 7. CSA measurements of water **(a)**, milk **(b)** and honey **(c)** droplets on LIS topographies before and after subjecting them to vibrations; **(d)** Images showing small 'satellite' droplets left behind by the milk droplet on MS-LIS topographies of PP and PS after the vibration test.

3.3.2 Shear assessments

The depletion of lubricant due to shear forces is another possible mode of LIS failures. The shear-induced loss of lubricant and its subsequent influence on LIS functionality was studied by subjecting the lubricant infused surfaces to shear, especially by continuous dripping of

droplets on a single track as shown in Fig. 8a. Only LIS topographies on PP substrates were investigated due to their shedding properties against milk and honey at lower tilt angles compared to their PS counterparts. Figs. 8b and c show sliding velocities of milk and honey droplets as a function of the increasing number of droplets dripped consecutively one after another. It is apparent from this figure that the milk droplet velocity decreased gradually on both MS-LIS and LIPSS-LIS substrates before reaching zero. However, the LIPSS topographies had shown to endure a greater number of droplets than the MS topographies. The velocity decrease can be explained with the interaction between the wetting ridge and capillary suction that led to lubricant redistribution as a result of the liquid droplet train on LIS and thus to the loss of the lubricant [46]. In particular, the shear forces caused by the droplet train led to a lubricant redistribution along the interconnected valleys of the MS topographies, especially towards the end of the tracks [31]. This phenomenon is illustrated by the gradual shade of the track in Fig. 8a. In addition, there was a lubricant deprivation at the beginning of the track which led to pinning of the droplet on the surface. The continuous loss of lubricant with each droplet detrimentally affected the LIS slippery properties, which was evident from the decreasing droplets velocity. At the same time, the velocity of honey droplets decreased rapidly on both LIPSS-LIS and MS-LIS substrates. Thus, the viscosity contrast at the liquid-lubricant interface in the case of honey was higher than that of milk and therefore the lubricant depletion could have been quicker in the case of honey. Such shear-induced loss was in line with what was previously reported, especially that the greater contrast between the working liquid and lubricant had a substantial impact on the LIS lubricant depletion [47]. Overall, the LIPSS-LIS topographies showed a better resistance than MS-LIS ones in regards to the effects of shear forces on the lubricant depletion.

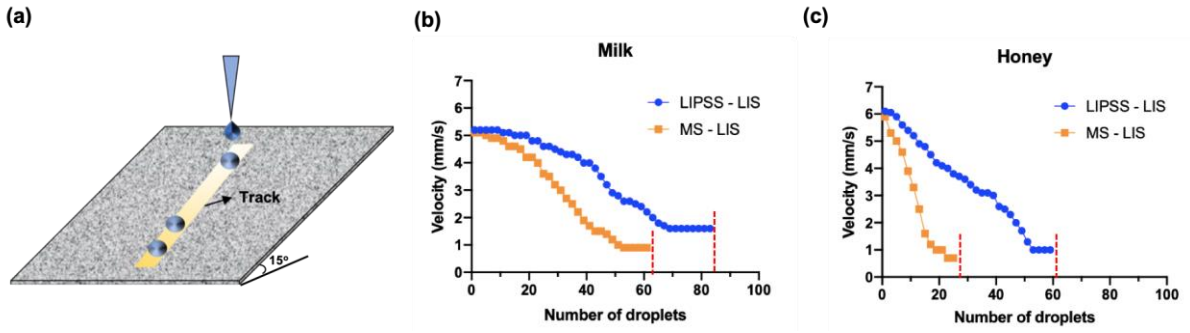

Figure 8. Analysis of lubricant depletion due to shear forces: **(a)** an illustration of the shear test performed on LIS topographies; the variations of sliding velocity with the increasing

number of milk **(b)** and honey **(c)** droplets on the PP surfaces with LIS topographies. **Note:** the red lines show the position where droplet velocity reached zero abruptly.

3.3.3 Immersion assessments

The LIS substrates were also investigated for their performance when exposed to bulk liquids. Fig. 9a shows the shedding behaviour of LIS on PP substrates exposed to honey and ketchup droplets of 250 µL. As it can be seen, the honey and ketchup droplets left behind traces on the as-received PP sheets, while LIS of the textured PP substrates exhibited an excellent anti-adhesive functionality. Thus, it is evident that LIS shed away not only viscous Newtonian liquids such as milk and honey but also yield stress liquids such as ketchup. In addition, the performance of thermoplastic-based LIS was investigated by conducting 50 dipping cycles into milk and honey. The honey was observed to stick to the as-received PS and PP sheets, however, their LIS counterparts resisted to any adhesion even after 25 cycles as shown in Fig.9b. The LIPSS-LIS treatment of both thermoplastics led to excellent anti-adhesive properties even after 50 cycles with all tested liquids, while there was a slight stickiness on the MS-LIS substrates after 43 and 20 dipping cycles in milk and honey, respectively. Especially, a similar behaviour such as small 'satellite' droplets was observed on both MS-LIS treated thermoplastics after the milk dipping cycles, whereas only small areas of MS-LIS had shown to lose their functionality after exposing them continuously to honey.

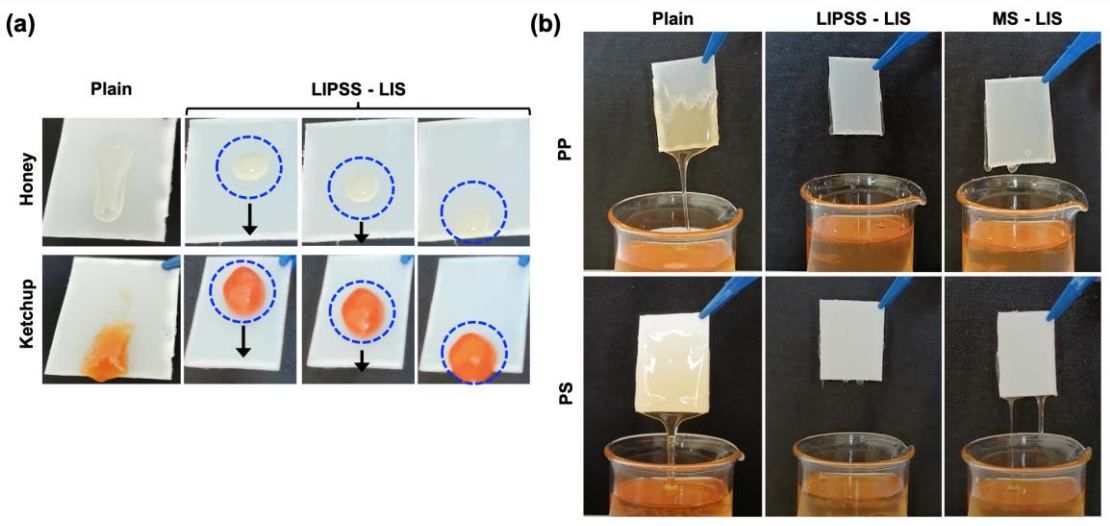

Figure 9. Analysis of the shedding behaviour of lubricant infused textured substrates: **(a)** the sliding behaviour of 250 µL honey and ketchup droplets on as-received and LIPSS - LIS treated

PP; **(b)** the dripping behaviour of as-received and LIPSS-LIS and MS-LIS treated PP and PS substrates after honey dipping cycles.

4. Conclusions

Lubricant impregnation of surfaces with micron/sub-micron topographies is a passive approach to achieve hydrophobic, lyophobic and lipophobic characteristics to surfaces. Such LIS exhibit greater stability and robustness than gas-cushioned textured surfaces because they usually fail under pressure- and/or dissolution-induced wetting instabilities. However, the LIS are also prone to other modes of failure such as vibration- and/or shear-induced instabilities. Surface topographies play an important role in overcoming such LIS failure mechanisms. The research investigated and experimentally validated the influence of different sub-micron (LIPSS) and multi-scale (MS) topographies fabricated by femtosecond laser processing on LIS functionality, especially in the context of their potential food packaging applications. The single scale, highly regular LIPSS topographies exhibited a better resistance to the lubricant depletion against vibration- and shear-induced forces when compared with their MS counterparts. Consequently, it was demonstrated that an ultrafine layer of lubricant on LIPSS topographies could also minimise the lubricant leaching as the result of interactions with different liquids when compared to MS topographies. Furthermore, the LIS treatment of thermoplastics used for food packaging led to excellent anti-adhesive characteristics when exposed to complex and highly viscous liquid foods. Although the highly regular LIPSS showed a reasonable robustness against various failure modes, further in-depth investigations are needed to optimise their functional response, especially by tailoring their geometry, depth and periodicity to improve their performance. Since most of the thermoplastic-based packaging solutions are fabricated by blow and injection moulding, the femtosecond laser treatment of replication masters as demonstrated in this research could be a seamless and cost-effective solution to “imprint” sub-micron topographies for preparing functional LIS with required durability.

Acknowledgements

The research work is supported by European Commission H2020 project ‘High-impact injection moulding platform for mass-production of 3D and/or large micro- structured surfaces with antimicrobial, self-cleaning, anti-scratch, anti-squeak and aesthetic functionalities”

(HIMALAIA). It is also conducted within the framework of UKIERI-DST programme on ‘Surface functionalisation for food, packaging, and healthcare applications’. The authors would like to acknowledge also the collaboration with LASEA SA, Belgium within the framework of the ESIF project “Smart Factory Hub” (SmartFub).

References

1. United Nations, 2019. Sustainable Development Goals. About the Sustainable Development Goals. New York: UN. [Online]. Available at: https://www.un.org/sustainabledevelopment/sustainable-development-goals/ [Accessed 10 January 2020].
2. Williams, H., Lindström, A., Trischler, J., Wikström, F. and Rowe, Z., 2020. Avoiding food becoming waste in households – The role of packaging in consumers’ practices across different food categories. *Journal of Cleaner Production*, *265*.
3. Djekic, I., Operta, S., Djulancic, N., Lorenzo, J.M., Barba, F.J., Djordjević, V. and Tomasevic, I., 2019. Quantities, environmental footprints and beliefs associated with household food waste in Bosnia and Herzegovina. Waste Management & Research, 37(12), pp. 1250-1260.
4. Williams, H., Wikström, F., Otterbring, T., Löfgren, M. and Gustafsson, A., 2012. Reasons for household food waste with special attention to packaging. *Journal of cleaner production*, *24*, pp.141-148.
5. Wohner, B., Pauer, E., Heinrich, V. and Tacker, M., 2019. Packaging-related food losses and waste: an overview of drivers and issues. *Sustainability*, *11*(1), p.264.
6. Liu, X., Wang, L., Qiao, Y., Sun, X., Ma, S., Cheng, X., Qi, W., Huang, W. and Li, Y., 2018. Adhesion of liquid food to packaging surfaces: Mechanisms, test methods, influencing factors and anti-adhesion methods. *Journal of Food Engineering*, *228*, pp.102-117.
7. Tuck, J.P., Alberini, F., Ward, D., Gore, B. and Fryer, P.J., 2020. Cleaning of thick viscoplastic surface deposits using an impinging jet: Effect of process variables. *Journal of Food Engineering*, *266*, p.109699.
8. Schaider, L.A., Balan, S.A., Blum, A., Andrews, D.Q., Strynar, M.J., Dickinson, M.E., Lunderberg, D.M., Lang, J.R. and Peaslee, G.F., 2017. Fluorinated compounds in US fast food packaging. *Environmental science & technology letters*, *4*(3), pp.105-111.

9. Eriksson, M., Claesson, P.M., Jarn, M., Tuominen, M., Wallqvist, V., Schoelkopf, J., Gane, P.A. and Swerin, A., 2019. Wetting Transition on Liquid-Repellent Surfaces Probed by Surface Force Measurements and Confocal Imaging. *Langmuir*, *35*(41), pp.13275-13285.
10. Gaddam, A., Agrawal, A., Joshi, S.S. and Thompson, M.C., 2015. Utilization of cavity vortex to delay the wetting transition in one-dimensional structured microchannels. *Langmuir*, *31*(49), pp.13373-13384.
11. Sharma, H., John, K., Gaddam, A., Navalkar, A., Maji, S.K. and Agrawal, A., 2018. A magnet-actuated biomimetic device for isolating biological entities in microwells. *Scientific reports*, *8*(1), pp.1-14.
12. Smith, J. D., Dhiman, R., Anand, S., Reza-Garduno, E., Cohen, R.E., McKinley, G.H. and Varanasi, K.K., 2013. Droplet mobility on lubricant-impregnated surfaces. *Soft Matter*, *9*(6), pp.1772-1780.
13. Van Buren, T. and Smits, A.J., 2017. Substantial drag reduction in turbulent flow using liquid-infused surfaces. *Journal of Fluid Mechanics*, *827*, pp.448-456.
14. Sharma, H., Gaddam, A., Agrawal, A. and Joshi, S.S., 2019. Slip flow through microchannels with lubricant-infused bi-dimensional textured surfaces. *Microfluidics and Nanofluidics*, *23*(2), p.28.
15. Jing, X. and Guo, Z., 2019. Durable Lubricant-Impregnated Surfaces for Water Collection under Extremely Severe Working Conditions. *ACS applied materials & interfaces*, *11*(39), pp.35949-35958.
16. He, X., Cao, P., Tian, F., Bai, X. and Yuan, C., 2019. Infused configurations induced by structures influence stability and antifouling performance of biomimetic lubricant-infused surfaces. *Surface and Coatings Technology*, 358, pp.159-166.
17. Siddiquie, R.Y., Gaddam, A., Agrawal, A., Dimov, S.S. and Joshi, S.S., 2020. Anti-biofouling properties of femtosecond laser-induced sub-micron topographies on elastomeric surfaces. *Langmuir*, *36* (19), pp. 5349–5358
18. Yamazaki, T., Tenjimbayashi, M., Manabe, K., Moriya, T., Nakamura, H., Nakamura, T., Matsubayashi, T., Tsuge, Y. and Shiratori, S., 2019. Antifreeze Liquid-Infused Surface with High Transparency, Low Ice Adhesion Strength, and Antifrosting Properties Fabricated through a Spray Layer-by-Layer Method. *Industrial & Engineering Chemistry Research*, *58*(6), pp.2225-2234.
19. Zhang, M., Liu, Q., Chen, R., Chen, H., Song, D., Liu, J., Zhang, H., Li, R., Wang, Y. and Wang, J., 2018. Lubricant-infused coating by double-layer ZnO on aluminium and its anti-corrosion performance. *Journal of Alloys and Compounds*, *764*, pp.730-737.

20. Lee, J., Jiang, Y., Hizal, F., Ban, G.H., Jun, S. and Choi, C.H., 2019. Durable omniphobicity of oil-impregnated anodic aluminum oxide nanostructured surfaces. *Journal of colloid and interface science*, *553*, pp.734-745.
21. Zouaghi, S., Bellayer, S., Thomy, V., Dargent, T., Coffinier, Y., Andre, C., Delaplace, G. and Jimenez, M., 2019. Biomimetic surface modifications of stainless steel targeting dairy fouling mitigation and bacterial adhesion. *Food and bioproducts processing*, *113*, pp.32-38.
22. Zhu, X., Lu, J., Li, X., Wang, B., Song, Y., Miao, X., Wang, Z. and Ren, G., 2019. Simple way to a slippery lubricant impregnated coating with ultrastability and self-replenishment property. *Industrial & Engineering Chemistry Research*, *58*(19), pp.8148-8153.
23. Li, Y., Bi, J., Wang, S., Zhang, T., Xu, X., Wang, H., Cheng, S., Zhu, B.W. and Tan, M., 2018. Bio-inspired edible superhydrophobic interface for reducing residual liquid food. *Journal of agricultural and food chemistry*, *66*(9), pp.2143-2150.
24. Li, Q. and Guo, Z., 2019. Lubricant-infused slippery surfaces: Facile fabrication, unique liquid repellence and antireflective properties. *Journal of colloid and interface science*, *536*, pp.507-515.
25. Rapoport, L., Solomon, B.R. and Varanasi, K.K., 2019. Mobility of Yield Stress Fluids on Lubricant-Impregnated Surfaces. *ACS applied materials & interfaces*, *11*(17), pp.16123-16129.
26. Yu, M., Liu, M., Hou, Y., Fu, S., Zhang, L., Li, M. and Wang, D., 2020. Facile fabrication of biomimetic slippery lubricant-infused transparent and multifunctional omniphobic surfaces. *Journal of Materials Science*, *55*(10), pp.4225-4237.
27. Wang, D., Guo, Z. and Liu, W., 2019. Bioinspired Edible Lubricant-Infused Surface with Liquid Residue Reduction Properties. Research, 2019, p.1649427.
28. Mukherjee, R., Habibi, M., Rashed, Z.T., Berbert, O., Shi, X. and Boreyko, J.B., 2018. Oil-Impregnated Hydrocarbon-Based Polymer Films. *Scientific reports*, *8*(1), pp.1-13.
29. Brown, P.S. and Bhushan, B., 2017. Liquid-impregnated porous polypropylene surfaces for liquid repellency. *Journal of colloid and interface science*, *487*, pp.437-443.
30. Brown, P.S. and Bhushan, B., 2017. Mechanically durable liquid-impregnated honeycomb surfaces. *Scientific reports*, *7*(1), pp.1-6.
31. Wexler, J.S., Jacobi, I. and Stone, H.A., 2015. Shear-driven failure of liquid-infused surfaces. *Physical review letters*, *114*(16), p.168301.

32. Baumli, P., Teisala, H., Bauer, H., Garcia-Gonzalez, D., Damle, V., Geyer, F., D'Acunzi, M., Kaltbeitzel, A., Butt, H.J. and Vollmer, D., 2019. Flow-Induced Long-Term Stable Slippery Surfaces. *Advanced science*, *6*(11), p.1900019.
33. Sartori, P., Guglielmin, E., Ferraro, D., Filippi, D., Zaltron, A., Pierno, M. and Mistura, G., 2019. Motion of Newtonian drops deposited on liquid-impregnated surfaces induced by vertical vibrations. *Journal of Fluid Mechanics*, *876*.
34. Romano, J.M., Garcia-Giron, A., Penchev, P. and Dimov, S., 2018. Triangular laser-induced submicron textures for functionalising stainless steel surfaces. *Applied Surface Science*, *440*, pp.162-169.
35. Trier, X., Taxvig, C., Rosenmai, A.K. and Pedersen, G.A., 2017. PFAS in paper and board for food contact: Options for risk management of poly-and perfluorinated substances.
36. Ribeiro-Santos, R., Andrade, M., de Melo, N.R. and Sanches-Silva, A., 2017. Use of essential oils in active food packaging: Recent advances and future trends. *Trends in food science & technology*, *61*, pp.132-140.
37. EFSA Panel on Food Additives and Flavourings (FAF), Younes, M., Aquilina, G., Castle, L., Engel, K.H., Fowler, P., Frutos Fernandez, M.J., Fürst, P., Gürtler, R., Gundert-Remy, U. and Husøy, T., 2020. Re-evaluation of dimethyl polysiloxane (E 900) as a food additive. *EFSA Journal*, *18*(5), p.e06107.
38. McHale, G., Orme, B.V., Wells, G.G. and Ledesma-Aguilar, R., 2019. Apparent Contact Angles on Lubricant-Impregnated Surfaces/SLIPS: From Superhydrophobicity to Electrowetting. *Langmuir*, *35*(11), pp.4197-4204.
39. Tan, B. and Venkatakrishnan, K., 2006. A femtosecond laser-induced periodical surface structure on crystalline silicon. *Journal of Micromechanics and Microengineering*, *16*(5), p.1080.
40. Gnilitskyi, I., Derrien, T.J.Y., Levy, Y., Bulgakova, N.M., Mocek, T. and Orazi, L., 2017. High-speed manufacturing of highly regular femtosecond laser-induced periodic surface structures: physical origin of regularity. *Scientific reports*, *7*(1), pp.1-11.
41. Lutey, A.H., Gemini, L., Romoli, L., Lazzini, G., Fuso, F., Faucon, M. and Kling, R., 2018. Towards laser-textured antibacterial surfaces. *Scientific reports*, *8*(1), pp.1-10.
42. Sciancalepore, C., Gemini, L., Romoli, L. and Bondioli, F., 2018. Study of the wettability behavior of stainless steel surfaces after ultrafast laser texturing. *Surface and Coatings Technology*, *352*, pp.370-377.
43. Garcia-Giron, A., Romano, J.M., Batal, A., Dashtbozorg, B., Dong, H., Solanas, E.M., Angos, D.U., Walker, M., Penchev, P. and Dimov, S.S., 2019. Durability and wear

resistance of laser-textured hardened stainless steel surfaces with hydrophobic properties. *Langmuir*, *35*(15), pp.5353-5363.

44. Xu, H., Clarke, A., Rothstein, J.P. and Poole, R.J., 2018. Viscoelastic drops moving on hydrophilic and superhydrophobic surfaces. *Journal of colloid and interface science*, *513*, pp.53-61.
45. Varagnolo, S., Mistura, G., Pierno, M. and Sbragaglia, M., 2015. Sliding droplets of xanthan solutions: a joint experimental and numerical study. *The European Physical Journal E*, *38*(11), p.126.
46. Kreder, M.J., Daniel, D., Tetreault, A., Cao, Z., Lemaire, B., Timonen, J.V. and Aizenberg, J., 2018. Film dynamics and lubricant depletion by droplets moving on lubricated surfaces. *Physical Review X*, *8*(3), p.031053.
47. Liu, Y., Wexler, J.S., Schönecker, C. and Stone, H.A., 2016. Effect of viscosity ratio on the shear-driven failure of liquid-infused surfaces. *Physical Review Fluids*, *1*(7), p.074003.